Priority Report

Cancer Research

The Distinctive Mutational Spectra of Polyomavirus-Negative Merkel Cell Carcinoma

Paul William Harms[1,2,3], Pankaj Vats[1,4], Monique Elise Verhaegen[3], Dan R. Robinson[1], Yi-Mi Wu[1,2], Saravana Mohan Dhanasekaran[1,2], Nallasivam Palanisamy[1,2,5], Javed Siddiqui[1,2], Xuhong Cao[1,6], Fengyun Su[1], Rui Wang[1,2], Hong Xiao[1,2,5], Lakshmi P. Kunju[1,2], Rohit Mehra[1,2,5], Scott A. Tomlins[1,2,7,8], Douglas Randall Fullen[2,3], Christopher Keram Bichakjian[3], Timothy M. Johnson[3], Andrzej Antoni Dlugosz[3,9], and Arul M. Chinnaiyan[1,2,6,7,8]

Abstract

Merkel cell carcinoma (MCC) is a rare but highly aggressive cutaneous neuroendocrine tumor. Merkel cell polyomavirus (MCPyV) may contribute to tumorigenesis in a subset of tumors via inhibition of tumor suppressors such as retinoblastoma (*RB1*) by mutated viral T antigens, but the molecular pathogenesis of MCPyV-negative MCC is largely unexplored. Through our MI-ONCOSEQ precision oncology study, we performed integrative sequencing on two cases of MCPyV-negative MCC, as well as a validation cohort of 14 additional MCC cases ($n = 16$). In addition to previously identified mutations in *TP53*, *RB1*, and *PIK3CA*, we discovered activating mutations of oncogenes, including *HRAS* and loss-of-function mutations in *PRUNE2* and *NOTCH* family genes in MCPyV-negative MCC. MCPyV-negative tumors also displayed high overall mutation burden (10.09 ± 2.32 mutations/Mb) and were characterized by a prominent UV-signature pattern with C > T transitions comprising 85% of mutations. In contrast, mutation burden was low in MCPyV-positive tumors (0.40 ± 0.09 mutations/Mb) and lacked a UV signature. These findings suggest a potential ontologic dichotomy in MCC, characterized by either viral-dependent or UV-dependent tumorigenic pathways. *Cancer Res; 75(18); 3720–7. ©2015 AACR.*

Introduction

Merkel cell carcinoma (MCC), or primary cutaneous neuroendocrine carcinoma, is a rare malignancy with high rates of recurrence, metastasis, and mortality. The incidence of MCC has nearly tripled in the past 20 years, and is more prevalent in the immunosuppressed and elderly. Five-year overall survival from time of diagnosis is 30% to 64% (1, 2). Previous studies to elucidate the molecular pathogenesis of MCC found that a subset of cases display *TP53*-inactivating mutations (14%–28%) and/or *PIK3CA*-activating mutations (4%–17%; ref. 1). The discovery of Merkel cell polyomavirus (MCPyV) viral DNA via digital subtraction transcriptome analysis in a majority of MCCs represented a major breakthrough (3). MCPyV may likely contribute to tumorigenesis via large T antigen (LTAg) inhibition of the tumor-suppressor RB1, and enhanced oncoprotein gene stability and mTOR activation by small T antigen (sTAg; refs. 1, 2). In MCC, MCPyV displays genomic integration and characteristic truncating mutations of LTAg, which render the virus replication deficient but preserve the RB-binding site (1, 3). In contrast, oncogenic activation events in MCPyV-negative MCC have been underexplored. No targeted therapies are currently available for MCC, although survivin, PI3K, and BCL2 inhibitors may hold promise (1, 4).

Next-generation sequencing (NGS) is a powerful, unbiased approach for identifying novel genetic aberrations in cancer, including point mutations, copy-number gains/losses, gene fusions, and viral sequences (5).Integrative sequencing incorporates data from whole-exome sequencing and whole-transcriptome sequencing to generate a comprehensive landscape of underlying genetic aberrations and outlier gene-expression changes in tumors (5). Recent exome sequencing studies on small cohorts of formalin-fixed, paraffin-embedded (FFPE) MCC samples identified recurrent *RB1* mutations in MCPyV-negative tumors, as well as *PDE4DIP* mutations (6, 7). However, NGS studies of MCC have, thus, far been limited, and detailed somatic mutation and expression analyses of MCC by integrative sequencing have not been reported.

The objective of the MI-ONCOSEQ precision oncology study is to carry out integrative sequencing of tumors from patients with

[1]Michigan Center for Translational Pathology, University of Michigan Medical School, Ann Arbor, Michigan. [2]Department of Pathology, University of Michigan Medical School, Ann Arbor, Michigan. [3]Department of Dermatology, University of Michigan Medical School, Ann Arbor, Michigan. [4]Department of Biomedical Science, Bharathidasan University, Tiruchirappalli, India. [5]Department of Urology, Henry Ford Health System, Detroit, Michigan. [6]Howard Hughes Medical Institute, University of Michigan Medical School, Ann Arbor, Michigan. [7]Comprehensive Cancer Center, University of Michigan Medical School, Ann Arbor, Michigan. [8]Department of Urology, University of Michigan Medical School, Ann Arbor, Michigan. [9]Department of Cell and Developmental Biology, University of Michigan Medical Center, Ann Arbor, Michigan.

Note: Supplementary data for this article are available at Cancer Research Online (http://cancerres.aacrjournals.org/).

P.W. Harms and P. Vats contributed equally to this article.

Corresponding Author: Arul M. Chinnaiyan, University of Michigan, 1400 East Medical Center Drive, 5316 CCGC 5940, Ann Arbor, MI 48109-5940. Phone: 734-615-4062; Fax: 734-615-4055; E-mail: arul@umich.edu

doi: 10.1158/0008-5472.CAN-15-0702

rare or refractory disease toward the goal of identifying novel therapeutic strategies (5). Here, we performed integrative sequencing of biospecimens obtained from two patients with MCC enrolled in the MI-ONCOSEQ study as well as a validation cohort of 14 MCC tumor samples.

Materials and Methods

Clinical study and tumor sample procurement

Patient samples were procured and profiled under Institutional Review Board (IRB)-approved studies. For MI-ONCOSEQ samples, patients were enrolled and consented through a University of Michigan Hospital System (UMHS) IRB-approved protocol for integrative tumor sequencing, MI-ONCOSEQ (IRB#HUM00046018). Specimen collection through MI-ONCOSEQ has been previously described (5), with tumor purity confirmed on frozen sections by the study pathologists (L.P. Kunju or S.A. Tomlins). Additional samples were procured from the UMHS Cutaneous Surgery and Oncology Program Tumor Bank, as previously described (8), with tumor purity of >70% confirmed on frozen section by the study dermatopathologists (D.R. Fullen or P.W. Harms). For tumor bank specimens, matched normal DNA was extracted from FFPE lymph node tissue using the QIAmp FFPE DNA Extraction Kit. All cases showed classic MCC immunophenotype, including expression of cytokeratin-20 and neuroendocrine marker(s). Sample details, including age, gender, and disease stage are summarized in Supplementary Table S1.

Preparation of NGS libraries

In this study, we generated 59 NGS libraries to characterize a total of 16 MCC patients from two different cohorts, namely MiOncoseq index cases and the validation cohort (Supplementary Tables S1 and S2). Exome libraries of tumor and matched normal genomic DNA and tumor RNA were generated using the Illumina TruSeq DNA Sample Prep Kit. RNA-seq libraries were prepared according to Illumina's TruSeq RNA protocol, using 2 μg total RNA, as previously described (9). Following standard quality control measures, libraries were analyzed by RNAseq (polyA-transcriptome), exome capture-transcriptome, and/or exome capture-genome sequencing (Supplementary Table S1). Paired-end libraries were sequenced with the Illumina HiSeq 2000. Reads that passed the Illumina BaseCall software chastity filter were used for subsequent analysis. Sequence and alignment quality were assessed by FastQC and the Picard package, respectively. Whole-exome library quality parameters are described in Supplementary Table S2.

Sequencing data analyses

Paired-end whole Exome fastq sequence files generated by Illumina (2000/2500) were aligned using Novoalign multi-threaded (version 2.08.02, Novocraft) to GRCh37 genome build. Post-processing of bam files generated by Novoalign were carried out using SAMtools (version 0.1.19; ref. 10) and Picard (version 1.93). Mutational analysis was carried out on matched normal–tumor pairs using VarScan2 algorithm (Version 2.3.2; ref. 11). The vcf files for somatic mutation were created with SNV positions having base quality phred score of at least q20, ×10 coverage in normal, less than 5% allelic fraction in 1000 Genomes, and at least 10 variant reads with two reads in each strand in the tumor library. SNVs with >5 recurrences reported in the Catalog of Somatic Mutations in Cancer (COSMIC) were also nominated to probe for known recurrent hotspot mutations. Indel analysis was carried out using Pindel (version 0.2.5). Candidate indels were further filtered by the homopolymer/repeat regions, recurrent sequencing artifacts in our compendia ($N = 800$), and high recurrence in 1000 Genomes, followed by manual curation. Nominated indels and SNV vcf's were then annotated using ANNOVAR package. Copy-number aberrations were quantified and reported for each gene as the copy-number ratio between each tumor and its matched normal sample, with minimum copy-number ratio cutoffs of 1.25 for gains or 0.75 for losses, as previously described (12). Copy-number analysis was performed only on index cases due to high duplication rates in some libraries of the validation cohort. Tumor content was analyzed as previously described (9).

Gene fusion and gene-expression analyses were carried out using Tuxedo suite tools [Tophat 2.0.4; ref. 13 and Bowtie (version 0.12.8)], using the "—fusion-search" option to find candidate fusions. Nominated fusions were manually inspected for annotation and ligation artifacts. Junction reads supporting fusion candidates were realigned using the BLAT alignment tool to confirm fusion breakpoints. Gene-expression analysis was performed on the accepted_hits.bam generated by Tophat as an input for the Cufflinks (version 2.0.2; ref. 14), which performs assembly of transcripts and estimates abundance in the transcriptome library. In addition, 56,369 transcripts from the Ensembl resource (Ensembl 66) were used as an annotation reference to quantify expression of individual transcripts and isoforms, as previously described (9). Unmapped sequences were used for downstream viral screening analysis using Bowtie and BLAT to align reads to all known viral genomes. Sequencing data for MIONCOSEQ cases will be deposited in dbGaP (accession: phs000673.v1.p1).

Statistical comparisons of mutation rates and C > T fraction were performed using the Student *t* test with Welch correction on GraphPad Prism 6 software.

Somatic mutation validation

NOTCH1-4, *PRUNE2*, *GRIN2A*, and *HRAS* somatic mutations were validated by Sanger sequencing at the University of Michigan Sequencing Core following PCR amplification. Because of limitations in frozen tissue availability, DNA for Sanger validation was extracted from archival FFPE tumor material for all cases except MO_1160, METMCC_862, and MCC345. Chromatograms were visualized using Sequence Scanner 2 software.

MCPyV detection

MCPyV copy number was quantitated by LT2 (LTAg) and SET9 (sTAg) qPCR of MCC tumor DNA along with the MKL-2 cell line as the standard as previously described (Supplementary Table S1; refs. 4, 15, 16). One sample with extremely low viral copy number (0.0006 copies/cell) was classified as MCPyV-negative, consistent with the precedent established by the previous MCC sequencing study (6). In cases with adequate tissue, MCPyV LTAg was detected by IHC with CM2B4 as previously described (15). One sample (METMCC_614) was positive for MCPyV by qPCR but negative by IHC. PCR-Sanger sequencing of LTAg was performed for this sample as previously described (15), which detected a tumor-specific truncating mutation; therefore, this tumor was classified as MCPyV positive.

Results and Discussion

Two patients with MCC were enrolled in the MI-ONCOSEQ precision medicine program. The first index patient (MO_1109) was a 60-year-old male who presented with MCC on the scalp that was treated with resection and adjuvant radiotherapy. After initial remission, the patient developed extensive metastatic disease that progressed despite chemotherapy. The patient was enrolled in MI-ONCOSEQ and underwent a biopsy of a chest wall metastasis (Fig. 1A). High-quality tumor RNA and DNA was subjected to NGS. There was no evidence of transcripts related to MCPyV or other oncogenic viruses; absence of MCPyV was confirmed by quantitative PCR, and therefore this tumor was considered

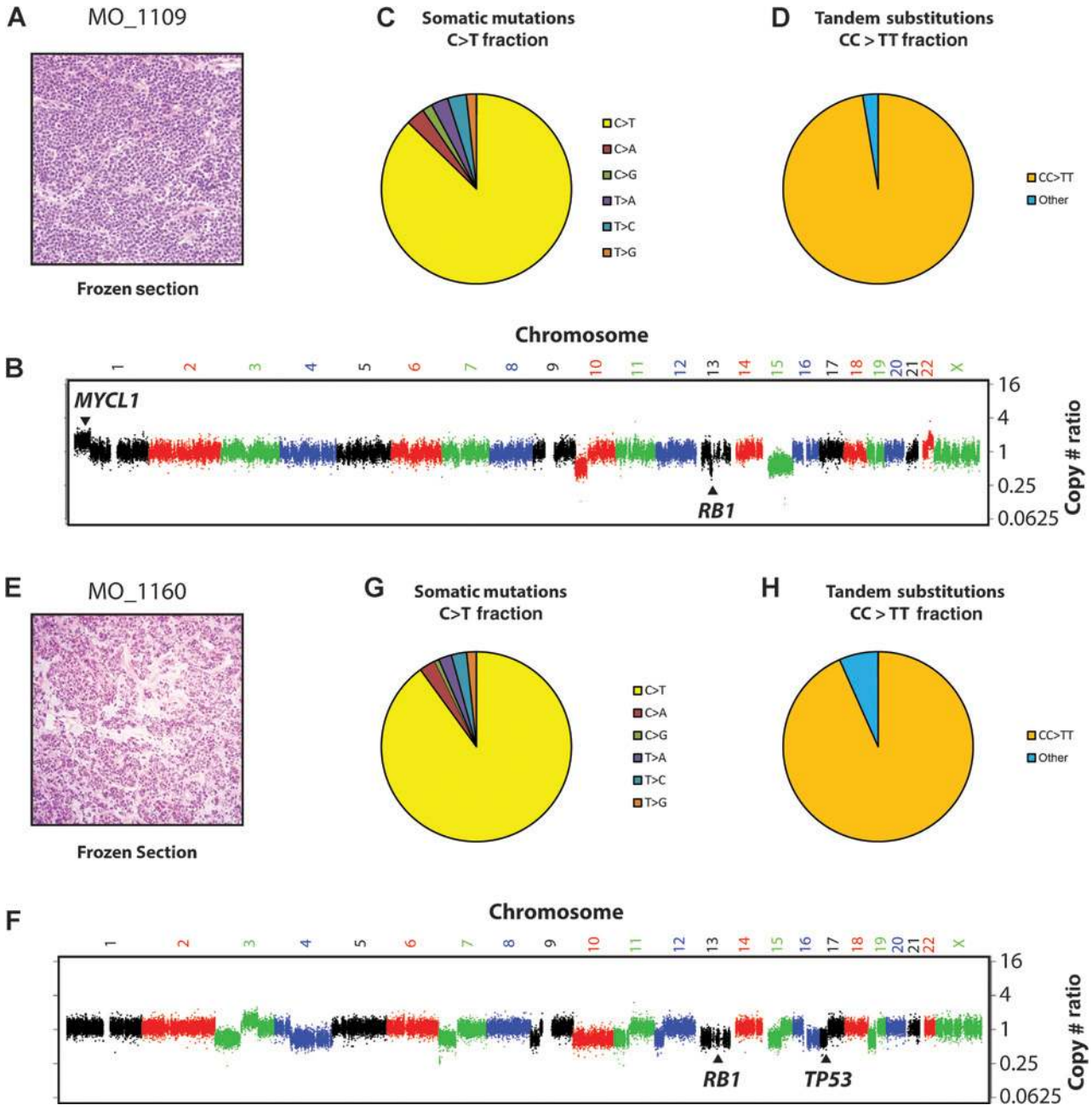

Figure 1.
NGS analysis of MCC index cases MO_1109 (A-D) and MO_1160 (E-H). A, frozen section of biopsy for MO_1109 demonstrating a round cell malignancy (hematoxylin and eosin, ×200). B, CNV in MO_1109, including copy gain at *MYCL1* and copy loss at *RB1*. C, somatic mutations in MO_1109 are dominated by C > T transitions. D, tandem substitutions in MO_1109 consist predominantly of CC > TT changes. E, frozen section of biopsy for MO_1160 demonstrating a round cell malignancy (hematoxylin and eosin, ×200). F, CNVs in MO_1160, including copy loss at *RB1* and *TP53*. G, somatic mutations in MO_1160 are dominated by C > T transitions. H, tandem substitutions in MO_1160 consist predominantly of CC > TT changes, consistent with UV-signature mutations.

MCPyV-negative (Supplementary Tables S1 and S3). In our copy-number variation (CNV) analysis, we detected 30 aberrations, including single copy loss of *RB1* and a single copy gain of chromosome 1p32.2-36.3 (region that includes *MYCL1*; Fig. 1B; Supplementary Table S4; ref. 17). The tumor harbored 1,084 nonsynonymous somatic exonic mutations, including a splice site mutation affecting the remaining copy of *RB1* (Supplementary Tables S5–S6). A predominance of cytosine to thymidine (C > T) transitions arising at dipyrimidine sites, or CC > TT tandem substitutions, is characteristic of the UV mutational signature (18). We next investigated the presence of such patterns in the SNV data and noted a high occurrence of C > T transitions (Fig. 1C; Supplementary Table S5). Examination of bases immediately 5′ and 3′ to mutated residues (18) revealed an enrichment of C > T transitions at dipyrimidine sites in MCC tumors, a pattern similar to the UV mutational signature in melanoma (Supplementary Fig. S1; ref. 18). The majority of tandem substitutions were CC > TT transitions, also consistent with UV-induced mutations (Fig. 1D; Supplementary Table S5).

The second index patient (MO_1160) was a 66-year-old male with a high-grade neuroendocrine tumor presenting in the parotid gland, favored to represent metastatic MCC of unknown primary. Metastases to bone, liver, and lymph nodes were present at diagnosis. The patient progressed despite radiotherapy and chemotherapy, and was subsequently enrolled in MIONCOSEQ. CT-guided needle biopsies were obtained from a liver metastasis (Fig. 1E). No evidence of oncogenic viruses was detected by NGS or MCPyV qPCR, leading us to conclude that the tumor was MCPyV negative. By CNV analysis, we detected 24 aberrations, including single-copy losses of *RB1*, *TP53*, and *PTEN* genes (Fig. 1F; Supplementary Table S4). Somatic mutation analysis revealed two *PIK3CA* mutations, including an activation hotspot E545K, and a P146S hotspot mutation in *TP53* (Supplementary Table S5). Similar to MO_1109, MO_1160 also demonstrated a high mutation burden (with a total of 1,441 nonsynonymous somatic mutation calls; Supplementary Table S5) dominated by C > T transitions characteristic of a UV-induced mutational signature (Fig. 1G; Supplementary Fig. S1; Supplementary Table S5). CC > TT changes dominated tandem substitutions, again consistent with UV-signature mutations from a cutaneous primary tumor (Fig. 1H). On the basis of the activating *PIK3CA* mutation in the patient's tumor, enrollment in a PI3K inhibitor trial was recommended during the Precision Medicine Tumor Board discussion.

We next expanded our analysis to a validation cohort of seven additional MCPyV-negative and seven MCPyV-positive MCC tumors, previously classified by qPCR for MCPyV status. Transcriptome libraries were queried for transcripts corresponding to known pathogens. MCPyV transcripts were identified in all tumors where MCPyV was detected by PCR (range of RNAseq viral read counts: 2,335–26,350; Supplementary Table S3). In addition, lower MCPyV reads (range, 39–46) were detected in two tumors that tested negative for MCPyV by PCR and IHC (Supplementary Table S3). Tumor-specific truncating LTAg mutations were not detected in mapped viral reads from these two tumors. Although this finding is of uncertain significance, the much lower number of viral reads in these two samples suggests background low-level viral loads previously reported in non-MCC carcinoma, possibly representing background wild-type viral infection (19). On the basis of the negative qPCR and IHC, these tumors were categorized as MCPyV negative. Other than MCPyV, no oncogenic pathogens were identified.

Across all MCC cases, we detected 5,351 total nonsynonymous mutations, of which 356 mutations were previously reported in the COSMIC database (Supplementary Table S6). MCPyV-negative tumors demonstrated markedly higher mutation rate per megabase than in MCPyV-positive tumors (mean 10.09 ± 2.32 vs. 0.40 ± 0.09, $P < 005$; Fig. 2A) and significantly higher C > T fraction (mean 0.86 ± 0.01 vs. 0.41 ± 0.03, $P < 0.0001$; Fig. 2B; Supplementary Table S5). In MCPyV-negative tumors, the majority (mean 92.7%) of tandem substitutions were CC > TT substitutions, with only 1 CC > TT tandem substitution (12.5%) detected across all MCPyV-positive tumors (Fig. 2C; Supplementary Table S5). As in the index cases, mutation signature analysis revealed enrichment of C > T transitions at dipyrimidine sites in MCPyV-negative MCC samples (Fig. 2D; Supplementary Fig. S1; ref. 18). There was no clear mutational signature in MCPyV-positive MCC samples (Supplementary Fig. S2). Mutation rate and C > T fraction were not significantly associated with patient age or primary tumor site. These findings support a molecular dichotomy in MCC with regard to viral status and mutational burden.

To identify mutations with likely functional significance, somatic mutation calls were ranked according to known activating oncogenic mutations and recurrent inactivating tumor-suppressor mutations (Fig. 3). We found MCC tumors to be heterogeneous with regard to candidate oncogenic drivers; however, MCPyV-negative tumors harbored highly recurrent tumor-suppressor mutations.

PIK3CA mutations were present in three tumors, two of which were activating (E545K and K111E; refs. 1, 20). Interestingly, in two cases, we also identified mutations novel to MCC in *KNSTRN*, a kinetochore gene recently reported to undergo oncogenic mutation in 19% of cutaneous squamous cell carcinomas (SCC; ref. 21). Similar to SCC, *KNSTRN* mutations in MCC resided in the N-terminus, including an S24F hotspot mutation. One MCPyV-positive tumor harbored two separate *HRAS* mutations (G12C and G13D) in distinct subclones (Supplementary Fig. S3 and Supplementary Tables S6–S7). *PIK3CA*, *KNSTRN*, and *HRAS* mutations were mutually exclusive in our cohort, suggesting a potential driver role in these samples. Four tumors harbored mutations in the oncogene *PREX2*, a negative regulator of PTEN. Activating mutations in *PREX2* are reported in 14% of melanomas (22). One tumor harbored *RAC1* (P29S)-activating mutation, a small G-protein mutated in melanoma (23). Overall, candidate oncogenic-activating mutations were identified in 6 of 8 (75%) and 2 of 7 (29%) of MCPyV-negative tumors and MCPyV-positive tumors, respectively.

MCPyV-negative tumors harbored several highly recurrent mutations in tumor-suppressor genes, including *TP53* (7/8, 87.5%), *RB1* (5/8, 62.5%), *NOTCH1* (4/8, 50%), and *PRUNE2* (5/8, 62.5%; Fig. 3; Supplementary Fig. S3, Supplementary Tables S6–S7). *PRUNE2* and *NOTCH1* mutations have not been described in MCC. *PRUNE2*, a proapoptotic factor (24), is mutated in 20% of melanomas (The Cancer Genome Atlas). We identified two inactivating mutations in the glutamate receptor subunit *GRIN2A* (2/8, 25%): A splice site mutation and the (R902K) loss-of-function mutation described in melanoma

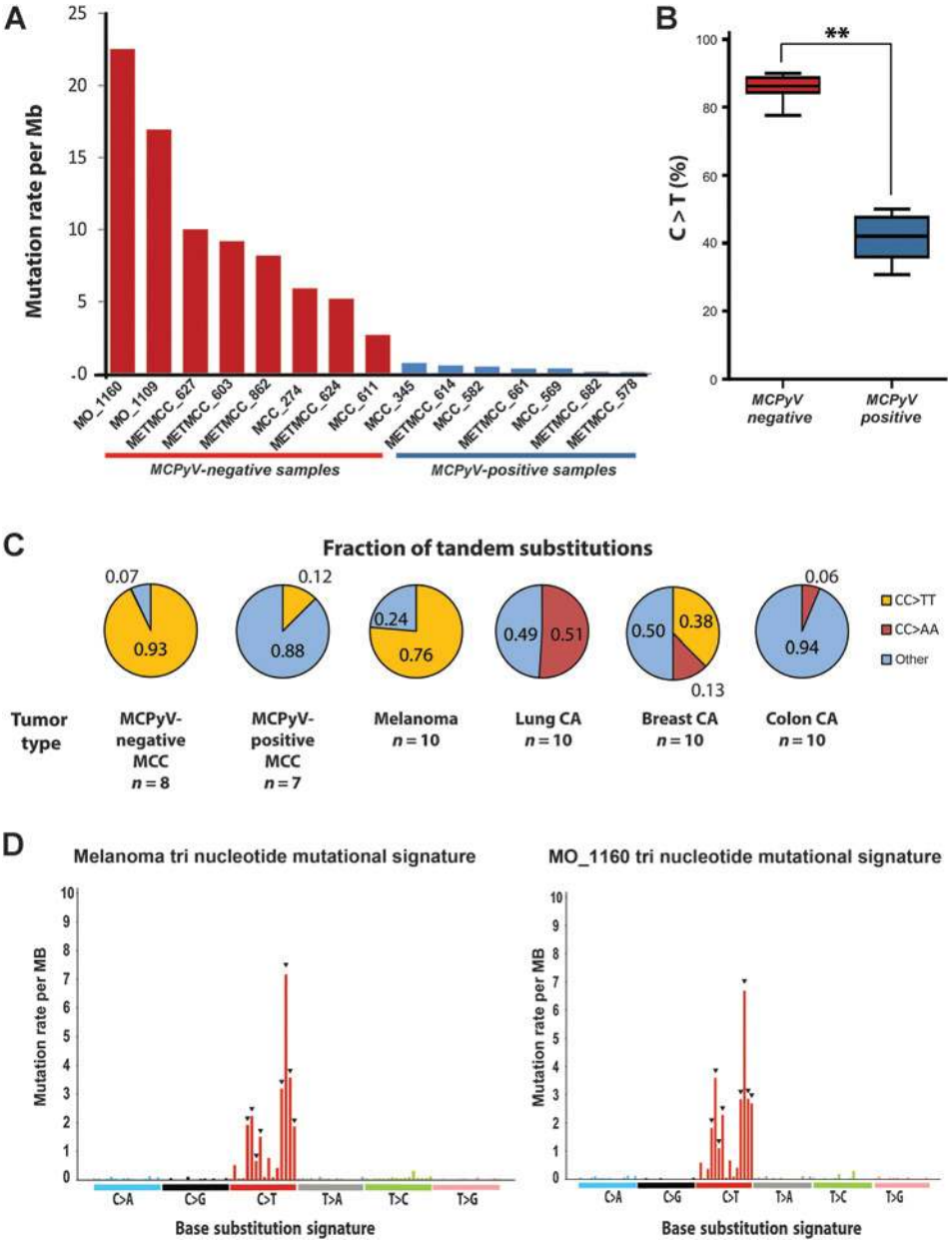

Figure 2.
Global mutation profiles of MCPyV-negative and MCPyV-positive MCC. A, significantly higher somatic mutation rate in MCPyV-negative tumors. B, C to T transitions are predominant in MCPyV-negative MCC, but not MCPyV-positive MCC; **, $P < 0.0001$. C, tandem substitutions are dominated by CC > TT changes (yellow) in melanoma and MCPyV-negative MCC. Other solid tumor types display predominantly CC > AA (red) or other changes (blue). For non-MCC tumors, profiles were generated from 10 randomly selected tumors of each type. D, trinucleotide mutation signatures demonstrate similar pattern of C to T transitions (red) in melanoma and a representative case of MCPyV-negative MCC. A randomly selected melanoma was used for comparison; arrowheads, C > T transitions at dipyrimidine sites. CA, carcinoma.

(Supplementary Tables S6–S7; ref. 25). Furthermore, we discovered a novel missense mutation in the DNA damage response gene *BRCA2* (D2819V) affecting the DNA-binding domain (Supplementary Table S6).

Interestingly, mutations affecting one or more *NOTCH* genes were identified in 6 of 8 (75%) MCPyV-negative MCCs (Fig. 3; Supplementary Tables S6–S7). *NOTCH* mutations in MCC were mainly located in EGF or ankyrin repeat regions, consistent with inactivating mutations (Fig. 4). We independently validated the somatic mutation calls by PCR-Sanger sequencing and confirmed the presence of *NOTCH* mutations in tumors, but not in the matched normal samples for 16 of 17 mutations (Supplementary Table S7). The majority of mutations were C > T transitions at dipyrimidine sites. Depending on cancer type, *NOTCH* signaling may play either an oncogenic or tumor-suppressor role (26, 27). In hematologic malignancies, *NOTCH* mutations or fusions that disrupt the C-terminal PEST domain result in increased *NOTCH* stability and aberrant signaling that promotes tumorigenesis. However, *NOTCH* signaling plays a tumor-suppressor role in SCC and small-cell lung carcinoma (26, 27). The clustering of *NOTCH* mutations in EGF and ankyrin repeat domains in our MCC cohort is consistent with loss-of-function events, suggesting that *NOTCH* signaling plays a tumor-suppressor role in MCC similar to other neuroendocrine malignancies.

Insertion/deletion analysis (indels) identified 32 indels (Supplementary Table S8). One tumor harbored an activating frameshift deletion at exon 6 in *PPM1D*, a negative regulator

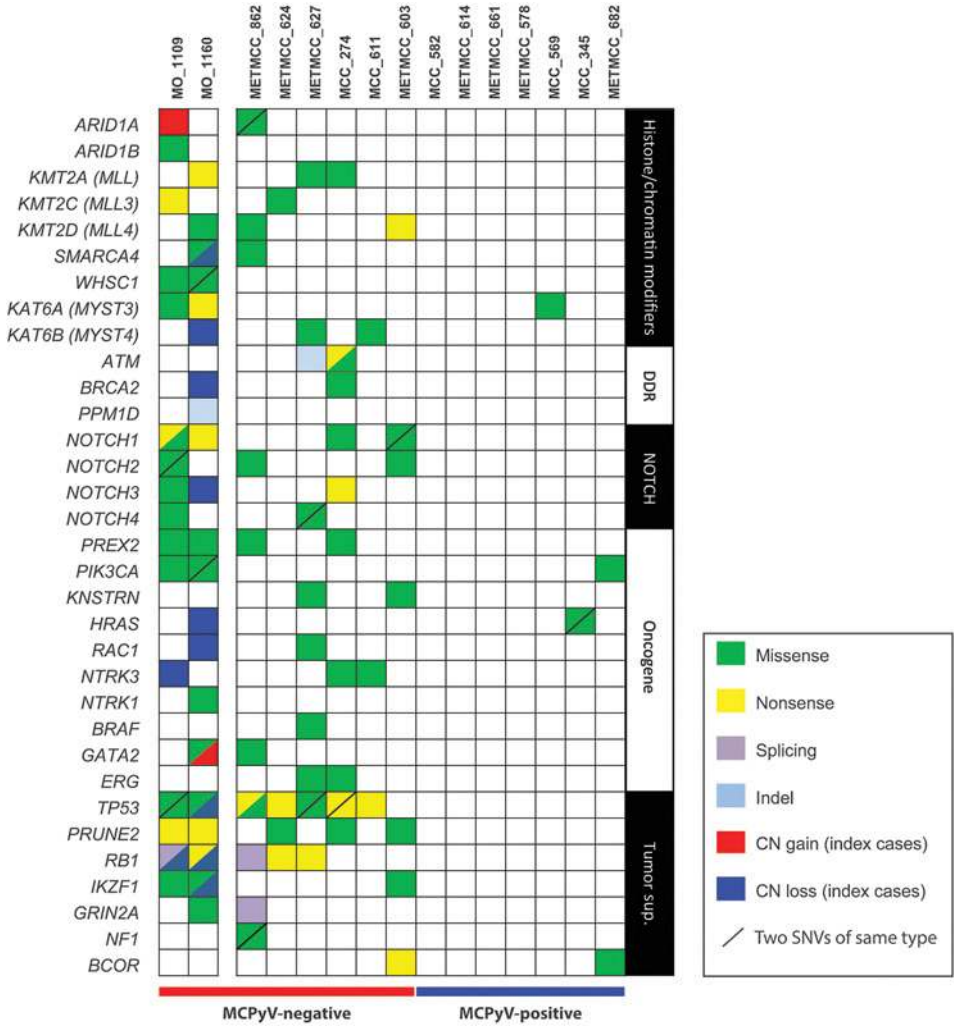

Figure 3.
Mutational landscape of MCPyV-negative and MCPyV-positive tumors. Green, missense mutations; yellow, nonsense mutations; light blue, indels; purple, splice site mutations; red, copy gain (index cases only); dark blue, copy loss (index cases only).

of p53 (28). Another tumor harbored a frameshift deletion of the DNA damage response gene *ATM* that is predicted to be inactivating due to loss of the kinase domain.

Fusion analysis revealed a total of 15 calls but no predicted oncogenic driver events were noted (Supplementary Table S9). However, we did identify a highly expressed fusion transcript in MCC_456 between *MLH1* and *SPATA4* (Supplementary Fig. S4A). This fusion results in loss of the C-terminal PMS2–EXO1 interaction domain of *MLH1*, a DNA mismatch repair gene, and has the potential to generate an inactive or dominant-negative form of the protein (Supplementary Fig. S4B). We independently confirmed this fusion by Sanger sequencing of the fusion PCR product from the index sample (Supplementary Fig. S4C). In addition, SPATA4 expression was restricted to the index sample, indicating 3′ partner expression driven by the underlying causal fusion event (Supplementary Fig. S4D–S4E). The functional significance of the fusion gene remains to be characterized.

Our studies found that MCCs segregate into distinct molecular classes; MCPyV-negative MCCs have high mutational burdens characterized by UV-signature events, supporting UV-induced damage as an etiology. In contrast, MCPyV-positive MCCs harbor relatively few mutations (25-fold lower than MCPyV-negative tumors) and do not display a definitive UV-signature, supporting an oncogenic role for MCPyV T antigens as primary drivers for these tumors. Our findings are analogous to those in head and neck SCCs, where tumors lacking human papillomavirus display higher mutation burdens (29). However, the observation that a minority of MCPyV-positive tumors harbor activating mutations in oncogenes such as *HRAS* suggests that genomic mutations may cooperate with the tumorigenic activity of MCPyV in some cases. MCPyV-negative MCCs harbored highly recurrent inactivation of candidate tumor suppressors, including *TP53*, *RB1*, *PRUNE2*, and *NOTCH1-4* genes. Our findings suggest that the NOTCH pathway plays a tumor-suppressor role in MCC. In contrast with tumor suppressors, MCCs are heterogeneous with regard to oncogenic drivers. The most frequently perturbed pathway was PI3K, with mutation of *PIK3CA* and/or *PREX2* identified in 5 of 15 (33%) tumors. *KNSTRN*, *RAC1*, and *HRAS* may represent novel oncogenic drivers in a subset of tumors. Altogether, our findings suggest that MCC

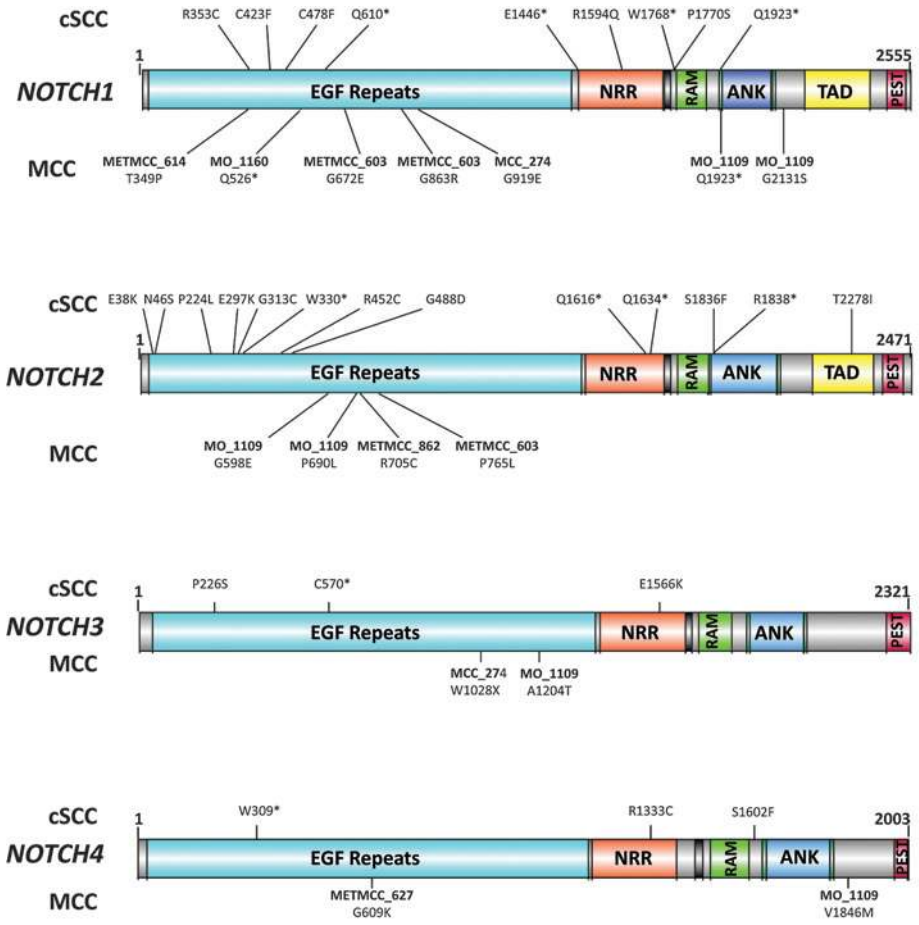

Figure 4.
Recurrent *NOTCH* family mutations in MCC. *NOTCH1-4* mutations in MCC cluster in EGF and ankyrin repeat domains, similar to tumor types with inactivating *NOTCH* mutations. Mutated codons above the diagram indicate previously described mutations in cutaneous SCC (27). EGF, epidermal growth factor–like motifs; ANK, Ankyrin repeats; TAD, transactivation domain; RAM, RBP-Jκ–associated module; PEST, protein domain enriched in proline, glutamic acid, serine, and threonine residues; cSCC, cutaneous squamous cell carcinoma; FPKM, fragments per kilobase of exon per million fragments mapped; CA, carcinoma.

pathogenesis can be molecularly divided into MCPyV-mediated and UV-mediated etiologies.

Disclosure of Potential Conflicts of Interest

No potential conflicts of interest were disclosed.

Authors' Contributions

Conception and design: P.W. Harms, P. Vats, R. Mehra, A.M. Chinnaiyan
Development of methodology: P.W. Harms, P. Vats, Y.-M. Wu, X. Cao, F. Su, R. Mehra
Acquisition of data (provided animals, acquired and managed patients, provided facilities, etc.): P.W. Harms, M.E. Verhaegen, D.R. Robinson, Y.-M. Wu, N. Palanisamy, J. Siddiqui, X. Cao, F. Su, H. Xiao, D.R. Fullen, C.K. Bichakjian, T.M. Johnson
Analysis and interpretation of data (e.g., statistical analysis, biostatistics, computational analysis): P.W. Harms, P. Vats, D.R. Robinson, Y.-M. Wu, S.M. Dhanasekaran, L.P. Kunju, S.A. Tomlins, A.A. Dlugosz
Writing, review, and/or revision of the manuscript: P.W. Harms, P. Vats, M.E. Verhaegen, Y.-M. Wu, S.M. Dhanasekaran, J. Siddiqui, L.P. Kunju, S.A. Tomlins, D.R. Fullen, C.K. Bichakjian, T.M. Johnson, A.A. Dlugosz, A.M. Chinnaiyan
Administrative, technical, or material support (i.e., reporting or organizing data, constructing databases): P.W. Harms, Y.-M. Wu, J. Siddiqui, R. Wang, H. Xiao
Study supervision: P.W. Harms, A.M. Chinnaiyan
Other (along with F. Su and R. Wang, prepared DNA and RNA, optimized the sequencing sample prep protocol and generated sequencing libraries, QC, and sequenced all the NGS samples, also helped to coordinate and manage the project): X. Cao
Other (consent, collect, annotate from charts, and distribute clinically annotated human samples from the skin cancer Biobank; direct and construct Biobank; review of article): T.M. Johnson

Acknowledgments

The authors acknowledge Jyoti Athanikar (writing and proofreading); Karen Giles (article submission); Dr. Michael Imperiale (assistance with response to reviewers); Jincheng Pan (assistance with initial fusion analysis); Angela Fullen, Lisa Johnson, and Mandy Davis (tissue microtomy); Nisha Meireles (tumor bank), Shannon Carskadon (PCR and IHC); and patients participating in the MI-ONCOSEQ clinical sequencing program and UMHS Cutaneous Surgery and Oncology Program. N. Palanisamy is a recipient of the Development Award from Melanoma Research Alliance. P.W. Harms is supported by the Dermatopathology Research Career Development Award of the Dermatology Foundation. S.A. Tomlins and A.M. Chinnaiyan are supported by the A. Alfred Taubman Medical Research Institute.

Grant Support

This project was supported in part by the Anatomic Pathology Project Funding Committee of the University of Michigan, Department of Pathology. The MI-ONCOSEQ study is funded by the NIH as a part of the National Human Genome Research Institute's Clinical Sequencing Exploratory Research program.

Received March 16, 2015; revised May 19, 2015; accepted July 1, 2015; published OnlineFirst August 3, 2015.

References

1. Erstad DJ, Cusack JCJr. Mutational analysis of merkel cell carcinoma. Cancers 2014;6:2116–36.
2. Bhatia S, Afanasiev O, Nghiem P. Immunobiology of Merkel cell carcinoma: implications for immunotherapy of a polyomavirus-associated cancer. Curr Oncol Rep 2011;13:488–97.
3. Feng H, Shuda M, Chang Y, Moore PS. Clonal integration of a polyomavirus in human Merkel cell carcinoma. Science 2008;319:1096–100.
4. Verhaegen ME, Mangelberger D, Weick JW, Vozheiko TD, Harms PW, Nash KT, et al. Merkel cell carcinoma dependence on bcl-2 family members for survival. J Invest Dermatol 2014;134:2241–50.
5. Roychowdhury S, Iyer MK, Robinson DR, Lonigro RJ, Wu YM, Cao X, et al. Personalized oncology through integrative high-throughput sequencing: a pilot study. Sci Transl Med 2011;3:111ra121.
6. Cimino PJ, Robirds DH, Tripp SR, Pfeifer JD, Abel HJ, Duncavage EJ. Retinoblastoma gene mutations detected by whole exome sequencing of Merkel cell carcinoma. Mod Pathol 2014;27:1073–87.
7. Graves CA, Jones A, Reynolds J, Stuart J, Pirisi L, Botrous P, et al. Neuroendocrine merkel cell carcinoma is associated with mutations in key DNA repair, epigenetic and apoptosis pathways: a case-based study using targeted massively parallel sequencing. Neuroendocrinology 2015;101:112–9.
8. Harms PW, Patel RM, Verhaegen ME, Giordano TJ, Nash KT, Johnson CN, et al. Distinct gene expression profiles of viral- and nonviral-associated merkel cell carcinoma revealed by transcriptome analysis. J Invest Dermatol 2013;133:936–45.
9. Robinson DR, Wu YM, Vats P, Su F, Lonigro RJ, Cao X, et al. Activating ESR1 mutations in hormone-resistant metastatic breast cancer. Nat Genet 2013;45:1446–51.
10. Li H, Handsaker B, Wysoker A, Fennell T, Ruan J, Homer N, et al. The Sequence Alignment/Map format and SAMtools. Bioinformatics 2009; 25:2078–9.
11. Koboldt DC, Zhang Q, Larson DE, Shen D, McLellan MD, Lin L, et al. VarScan 2: somatic mutation and copy-number alteration discovery in cancer by exome sequencing. Genome Res 2012;22:568–76.
12. Lonigro RJ, Grasso CS, Robinson DR, Jing X, Wu YM, Cao X, et al. Detection of somatic copy number alterations in cancer using targeted exome capture sequencing. Neoplasia 2011;13:1019–25.
13. Kim D, Salzberg SL. TopHat-Fusion: an algorithm for discovery of novel fusion transcripts. Genome Biol 2011;12:R72.
14. Trapnell C, Roberts A, Goff L, Pertea G, Kim D, Kelley DR, et al. Differential gene and transcript expression analysis of RNA-seq experiments with TopHat and Cufflinks. Nat Protoc 2012;7:562–78.
15. Fisher CA, Harms PW, McHugh JB, Edwards PC, Siddiqui J, Palanisamy N, et al. Small cell carcinoma in the parotid harboring Merkel cell polyomavirus. Oral Surg Oral Med Oral Pathol Oral Radiol 2014;118:703–12.
16. Rodig SJ, Cheng J, Wardzala J, DoRosario A, Scanlon JJ, Laga AC, et al. Improved detection suggests all Merkel cell carcinomas harbor Merkel polyomavirus. J Clin Invest 2012;122:4645–53.
17. Paulson KG, Lemos BD, Feng B, Jaimes N, Penas PF, Bi X, et al. Array-CGH reveals recurrent genomic changes in Merkel cell carcinoma, including amplification of L-Myc. J Invest Dermatol 2009;129:1547–55.
18. Alexandrov LB, Nik-Zainal S, Wedge DC, Aparicio SA, Behjati S, Biankin AV, et al. Signatures of mutational processes in human cancer. Nature 2013;500:415–21.
19. Fimereli D, Gacquer D, Fumagalli D, Salgado R, Rothe F, Larsimont D, et al. No significant viral transcription detected in whole breast cancer transcriptomes. BMC Cancer 2015;15:147.
20. Rudd ML, Price JC, Fogoros S, Godwin AK, Sgroi DC, Merino MJ, et al. A unique spectrum of somatic PIK3CA (p110alpha) mutations within primary endometrial carcinomas. Clin Cancer Res 2011;17:1331–40.
21. Lee CS, Bhaduri A, Mah A, Johnson WL, Ungewickell A, Aros CJ, et al. Recurrent point mutations in the kinetochore gene KNSTRN in cutaneous squamous cell carcinoma. Nat Genet 2014;46:1060–2.
22. Berger MF, Hodis E, Heffernan TP, Deribe YL, Lawrence MS, Protopopov A, et al. Melanoma genome sequencing reveals frequent PREX2 mutations. Nature 2012;485:502–6.
23. Krauthammer M, Kong Y, Ha BH, Evans P, Bacchiocchi A, McCusker JP, et al. Exome sequencing identifies recurrent somatic RAC1 mutations in melanoma. Nat Genet 2012;44:1006–14.
24. Machida T, Fujita T, Ooo ML, Ohira M, Isogai E, Mihara M, et al. Increased expression of proapoptotic BMCC1, a novel gene with the BNIP2 and Cdc42GAP homology (BCH) domain, is associated with favorable prognosis in human neuroblastomas. Oncogene 2006;25:1931–42.
25. Prickett TD, Zerlanko BJ, Hill VK, Gartner JJ, Qutob N, Jiang J, et al. Somatic mutation of GRIN2A in malignant melanoma results in loss of tumor suppressor activity via aberrant NMDAR complex formation. J Invest Dermatol 2014;134:2390–8.
26. Kunnimalaiyaan M, Chen H. Tumor suppressor role of Notch-1 signaling in neuroendocrine tumors. Oncologist 2007;12:535–42.
27. Wang NJ, Sanborn Z, Arnett KL, Bayston LJ, Liao W, Proby CM, et al. Loss-of-function mutations in Notch receptors in cutaneous and lung squamous cell carcinoma. Proc Natl Acad Sci U S A 2011;108: 17761–6.
28. Kleiblova P, Shaltiel IA, Benada J, Sevcik J, Pechackova S, Pohlreich P, et al. Gain-of-function mutations of PPM1D/Wip1 impair the p53-dependent G_1 checkpoint. J Cell Biol 2013;201:511–21.
29. Stransky N, Egloff AM, Tward AD, Kostic AD, Cibulskis K, Sivachenko A, et al. The mutational landscape of head and neck squamous cell carcinoma. Science 2011;333:1157–60.